Optimal Signal Averaging Time in VLBI Sessions

Yuriy Vekshin, Voytsekh Ken, Sergei Kurdubov

Abstract We propose a technique for determining an optimal averaging time of source signals in VLBI, taking into account signal delay instability in the radio telescope's equipment. Delay instability is determined by calculating fringe parameters over a continuous one-hour source tracking session. Optimal signal averaging time (which provides minimum error of delay measuring) is determined by calculating the Allan deviation. The delay measurement error increases at a longer averaging time due to delay instability. Source signal averaging time is determined in such a way that the delay's calculated standard deviation is not less than the radio telescope equipment's delay instability Allan deviation. The results of measuring delay instability of the RT-13 radio telescopes of the Quasar VLBI Network in the S-, X-, and Ka-bands were applied to R-X sessions postprocessing. Some previous sessions were recalculated by changing the scheduled source signal averaging time to an optimal one for more intensive sources. The comparison of the UT1-UTC determination and its formal errors obtained with scheduled averaging time and optimal averaging time is presented.

Keywords radio interferometer, VLBI, tri-band receiver, correlator, signal-to-noise ratio, group delay, delay stability, Universal Time

Institute of Applied Astronomy of the Russian Academy of Sciences (IAA RAS)

1 Introduction

The accuracy of Universal Time determination is greatly dependent on the group delay measurement accuracy of the radio interferometer. The measurement error of fringe delay depends on signal delay instability in radio telescope equipment [1]. It should be measured and taken into account when scheduling source scan times in VLBI-sessions.

The signal-to-noise ratio (*SNR*) of the radio interferometer at the correlator output is determined by the source flux F_s, system equivalent flux density (*SEFD*) of radio telescopes, quantization efficiency η, bandwidth Δf, and averaging time τ_a [2].

$$SNR = \frac{\eta \cdot F_s}{\sqrt{SEFD_1 \cdot SEFD_2}} \sqrt{2 \cdot \Delta f \cdot \tau_a}. \qquad (1)$$

Theoretical fringe delay error σ_{tSNR} depends only on SNR and bandwidth Δf [2].

$$\sigma_{tSNR} = \frac{\sqrt{12}}{2\pi \cdot \Delta f \cdot SNR}. \qquad (2)$$

Real fringe delay error σ_t depends on signal delay instability in radio telescope equipment σ_{tEq}, including receivers, acquisition systems, synchronization systems, etc.

$$\sigma_t = \sqrt{\sigma_{tSNR}^2 + \sigma_{tEq}^2}. \qquad (3)$$

2 Measurement Technique

To obtain signal delay instability, we have carried out a continuous one-hour tracking session of the cos-

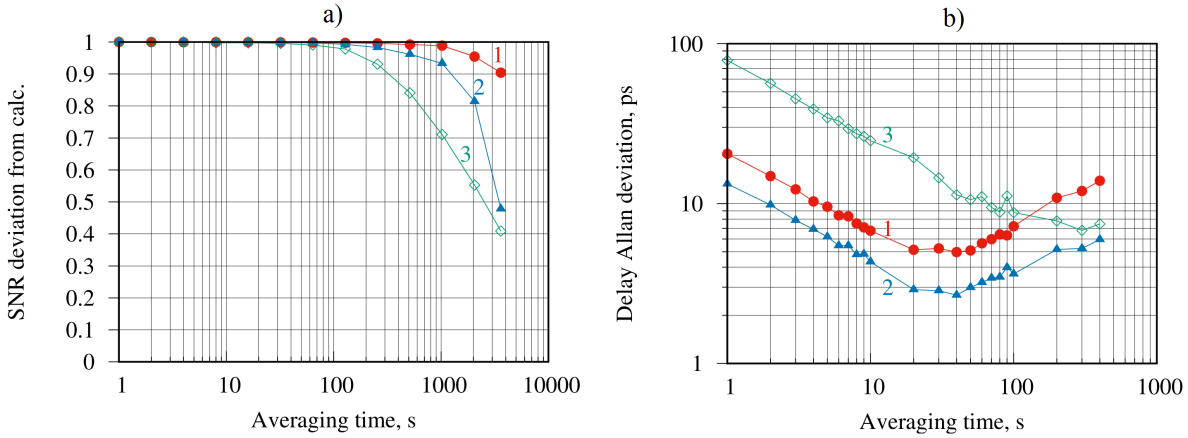

Fig. 1 a) Signal-to-noise ratio deviation from the calculated one; b) Delay Allan deviation for one-hour 3C454.3 tracking: 1–S-band, 2–X-band, 3–Ka-band.

mic source 3C454.3 by the RT-13 radio telescopes [3] at Badary, Zelenchukskaya, and Svetloe. Triband receivers with the S- (2.2–2.6 GHz), X- (7.0–9.5 GHz), and Ka- (28–34 GHz) bands [4] Broadband Acquisition System (Δf=512 MHz, 2 bit quantization) [5] were used. Signal-to-noise ratios and group delays at 1 s averaging time (3,600 points) were obtained by the RASFX correlator [6, 7]. The total geometric delays were calculated, ionospheric delays were taken into account, and NGS files were generated, which were further processed by the "Quasar" software [8]. O-C files were obtained, containing the differences between the observed and calculated delays.

The signal-to-noise ratio at the correlator output was then calculated at different averaging times (Figure 1, a). It was found that the SNR decreases by 10% from the value calculated by (1) at one hour for S-band, 1400 s for X-band, and 350 s for Ka-band due to frequency standards instability.

Then we have the calculated delay Allan deviation, and we found that delay instability appears at shorter time intervals (Figure 1, b). The Allan deviation decreases like white noise, proportional to the square root of the averaging time according to (1, 2) up to 20 s averaging time in the S- and X-bands and up to 200 s averaging time in Ka-band. It is an optimal averaging time, at which the minimum delay Allan deviation value is achieved. Radio telescope equipment instability prevails at longer averaging times. The minimum delay deviation is 5 ps in S-band, 3 ps in X-band, and 7 ps in Ka-band. White noise in Ka-band is greater than in the S/X-bands due to the lower signal-to-noise ratio, so the averaging time to reach the radio telescope equipment delay instability is longer. The first theoretical term of delay error (3) is the straight line on the Allan deviation plot in a log-log scale (Figure 1, b), and this line moves parallel along the y-axis depending on the source flux F_s according to (1) and (2). The second practical term of delay error (3) is the radio telescope equipment delay instability and is source independent. The intersection of these two terms gives the optimal averaging time for the source signal. So, each source has its own optimal averaging time. We propose to choose the averaging time of a source signal when scheduling VLBI-sessions in such a way that the delay's calculated standard deviation is not less than the radio telescope equipment's delay instability Allan deviation. A further increase in averaging time will give an increase in the delay measurement error (Figure 1, b).

3 Practical Application

We have tested this technique on the R-X sessions in the S/X/Ka-bands. As scheduled, the session lasts one hour and contains 22 scans with an averaging time of 120 s. The signal-to-noise ratio was measured for all sources, and the delay error was calculated by (2) in the S-, X-, and Ka-bands (Table 1).

The calculated delay error in X-band for some Intensive sources (1156+295, 1546+027, and NRAO150) is less than the real delay instability of 3 ps and, con-

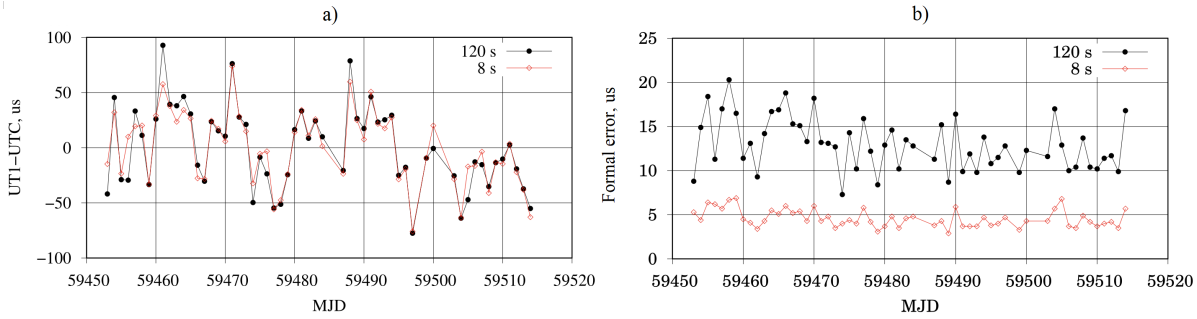

Fig. 2 X/S-band combination results: a) UT1-UTC differences with respect to the IERS finals series; b) formal errors (UT1-UTC).

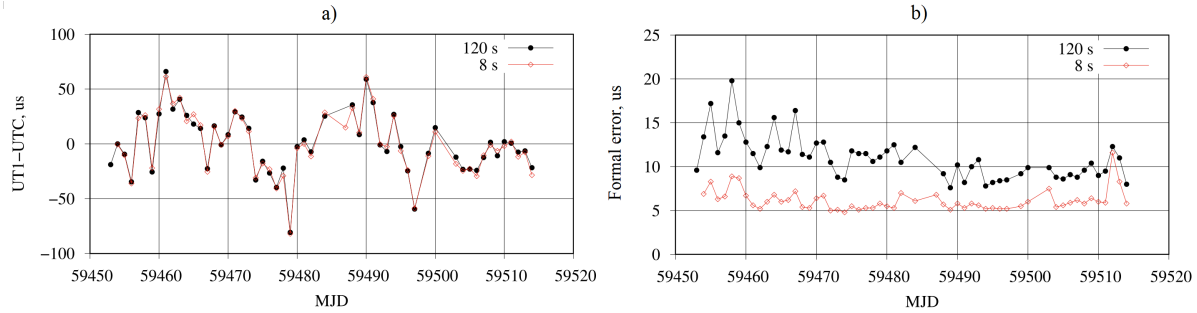

Fig. 3 Ka/X-band combination results: a) UT1-UTC differences with respect to the IERS finals series; b) formal errors (UT1-UTC).

Table 1 Measured SNR and calculated delay standard deviation in R-X sessions.

Source	Number of obs.	SNR (meas.)			σ_{tSNR}, ps (calc.)		
		S	X	Ka	S	X	Ka
1717+178	1	136	184	33	7.9	5.8	32.4
0642+449	1	122	198	41	8.8	5.4	26.3
1156+295	2	61	628	260	17.7	**1.7**	4.1
1642+690	1	122	165	18	8.8	6.5	61.0
1546+027	6	363	861	98	3.0	**1.3**	11.0
NRAO150	2	93	644	185	11.6	**1.7**	5.8
OK290	2	62	211	35	17.4	5.1	30.3
0716+714	6	85	201	36	12.6	5.4	29.8
0805+410	1	58	244	21	18.5	4.4	51.1

sequently, is not achieved in practice. So, the averaging time has been reduced for these Intensive sources. 120 s scans were cut into slices, and then all were processed.

The R-X sessions from a two month period (27.08.2021–27.10.2021) were processed with different averaging times for selected sources. The averaging times varied from 120 s to 8 s. UT1-UTC differences with respect to the IERS finals series and its formal errors were obtained by "Quasar" software [8] for X/S-band and Ka/X-band combinations. The second band is used to eliminate ionospheric delay. The formal error is the root mean square of residual errors after solving a system of equations by the least squares method.

UT1-UTC series and formal errors for the 120 s and 8 s averaging times are presented in Figure 2 for the X/S combination and in Figure 3 for the Ka/X combination. The standard deviations of the (UT1-UTC) series $\sigma_{UT1-UTC}$ and mean formal errors were calculated and are presented in Table 2.

Table 2 Standard deviations of (UT1-UTC) series residuals from IERS finals and its formal errors, in microseconds.

Aver. time, s	X/S-bands		Ka/X-bands	
	$\sigma_{UT1-UTC}$	Form. error	$\sigma_{UT1-UTC}$	Form. error
120	36.6	13.0	27. 2	11.0
60	35.1	10.6	27.4	9.5
30	34.5	8.1	27.3	8.0
15	33.7	5.9	27.4	6.8
8	32.4	4.6	27.7	6.1

Reducing the averaging time from 120 s to 8 s has led to reducing the standard deviation of the UT series by 4 μs and the formal error by 8 μs for the X/S com-

bination. Errors have decreased for the 8 s averaging time because white noise in the delay Allan deviation plot prevails over this interval for X-band (see plot 2 in Figure 1, b), and delay instability does not affect the measurement result; at longer averaging times, delay instability prevails. For Ka/X, the combination formal error has decreased by 5 μs at the 8 s averaging time. The standard deviation of the (UT1-UTC) series in Ka-band is almost independent on the averaging time from 120 s to 8 s, because there is white noise on the delay Allan deviation plot in Ka-band over these time intervals (see plot 3 in Figure 1, b). The standard deviation of UT1 corrections in regular two-hour R sessions in the S/X-bands with different scan times from 16 s to 60 s is about 20 μs.

4 Conclusions

The radio telescope's equipment delay instability should be taken into account in addition to the signal-to-noise ratio when scheduling VLBI-sessions. Long continuous source tracking and Allan deviation calculation should be used to obtain the delay instability of the radio interferometer. The optimal source signal averaging time is determined by the minimum of the delay Allan deviation plot in such a way that the delay's calculated standard deviation is not less than the radio telescope equipment's delay instability Allan deviation. Reducing the averaging time (cutting scans into slices) for Intensive sources leads to a decrease in UT determination errors, because instability does not affect the delay error at short time intervals. A change in scheduling, providing reduction of source scan times and an increase in the number of sources, should lead to a greater decrease in UT determination errors.

Acknowledgements

We are grateful to Alexey Melnikov, Svetlana Mironova, and Igor Surkis for their assistance and discussion of the results.

References

1. Y. Vekshin, V. Ken, V. Chernov, A. Evstigneev, E. Khvostov, M. Zotov. Analysis of VLBI Interferometer Characteristics Using Zero-baseline Lab Prototype and RASFX Correlator. *Proceedings of Science*, vol. 344, 142, 2019. doi:10.22323/1.344.0142.
2. A. R. Thompson, J. M. Moran, G. W. Swenson Jr. *Interferometry and Synthesis in Radio Astronomy*. Springer, 2017. doi:10.1007/978-3-319-44431-4.
3. D. Ivanov, A. Ipatov, D. Marshalov et.al. Russian New Generation VLBI Network. *IVS 2022 General Meeting Proceedings*, 2022, this volume.
4. A. A. Evstigneev, V. K. Chernov, O. Eu. Evstigneeva, I. A. Ipatova, Eu. Yu. Khvostov, A. P. Lavrov, I. A. Pozdnyakov, Yu. V. Vekshin, M. B. Zotov. RT-13 VLBI receivers. *Transactions of IAA RAS*, vol. 55, pp. 36–40, 2020. doi:10.32876/ApplAstron.55.36-40.
5. E. Nosov, D. Marshalov, A. Melnikov. Operating Experience with the Broadband Acquisition System on the RT-13 Radio Telescopes. *IVS 2016 General Meeting Proceedings "New Horizons with VGOS"*, edited by D. Behrend, K. Baver, and K. Armstrong, NASA/CP–2016–219016, pp. 53-57, 2016.
6. I. F. Surkis, V. F. Zimovsky, V. O. Ken et al. *Instrum Exp Tech*, 61, pp. 772-779, 2018. doi:10.1134/S0020441218060131.
7. V. O. Ken. Overview of RASFX: IAA RAS VLBI software correlator. *Transactions of IAA RAS*, vol. 55, pp. 41–44, 2020. doi:10.32876/ApplAstron.55.41-44.
8. S. L. Kurdubov, V. S. Gubanov. Main results of the global adjustment of VLBI observations. *Astron. Lett.*, 37 (4), pp. 267–275, 2011. doi:10.1134/S1063773711010063.